Biochemistry

 Volume 36, Number 2 January 14, 1997

Accelerated Publications

Femtosecond Transient Absorption Study of Carotenoid to Chlorophyll Energy Transfer in the Light-Harvesting Complex II of Photosystem II†

James P. Connelly,‡ Marc G. Müller,‡ Roberto Bassi,§ Roberta Croce,§ and Alfred R. Holzwarth*,‡

Max-Planck-Institut für Strahlenchemie, Stiftstrasse 34-36, D-45470 Mülheim an der Ruhr, Germany, and Biotechnologie Vegetali, Università di Verona, Strada Le Grazie, Verona I-37100, Italy

Received October 1, 1996; Revised Manuscript Received November 13, 1996⊗

ABSTRACT: Singlet energy transfer between the carotenoids (Cars) and chlorophylls (Chls) in the light-harvesting complex II (LHC II) from higher plants has been studied using ultrafast transient absorption spectroscopy by exciting the Cars directly in the 475−515 nm wavelength range. LHC II trimers from *Arabidopsis thaliana* with well-defined Car compositions have been used. From HPLC, the wild type (WT) monomer contains two luteins (Ls), one neoxanthin (N), and a trace of violaxanthin (V) per 12 Chls. The ABA-3 mutant contains 1.4 Ls and 0.6 zeaxanthin (Z) per monomer. Though exploitation of the difference in Car constitution and exciting the WT at 475 and 490 nm, and the ABA-3 mutant at 490 and 515 nm, the different Car contributions to energy transfer have been probed. Evidence for energy transfer mainly from the Car to Chl *b* is observed in the WT. In the mutant, additional transfer from Car to Chl *a* correlates with the presence of Z. The results imply predominant energy transfer from the central Ls to Chl *b* which requires a modification of the currently accepted arrangement of Chl pigments in LHC II.

As the most abundant and outermost antenna of photosystem (PS) II, light-harvesting complex (LHC)[1] II is involved in absorption and energy transfer mainly by means of chlorophyll (Chl) that paves the excitation transfer route to the reaction center (Jennings et al., 1996). Carotenoids (Cars) are also present and fulfill several functions (Frank & Cogdell, 1996). Nonphotochemical quenching mechanisms that control the efficiency of PS II (Horton et al., 1996; Ruban et al., 1996) are known to involve the xanthophyll cycle Cars, although the location of the most significant quenching processes appears to be predominantly associated with the minor antennas, i.e. CP 26 and 29 (Bassi et al., 1993; Bergantino et al., 1995). Rather, the Cars associated with LHC II probably serve both to prevent the formation of the Chl triplet state that can react with oxygen to form the damaging singlet oxygen (Peterman et al., 1995) and as antennas absorbing in the blue green spectral region and transferring singlet excitation to the Chls (Frank & Cogdell, 1996). The Cars are also vital for stabilizing the structure of LHC II, as demonstrated by the need for them in reconstituting LHC II (Paulsen, 1995).

The spectral properties of carotenoids, typical of those found in antenna complexes, have been studied quite

† This work was performed within the European Union HCM network (Contract CT940619) and was also supported in part by the Deutsche Forschungsgemeinschaft SFB 189, Heinrich-Heine-Universität Düsseldorf, and the Max-Planck-Institut für Strahlenchemie, Mülheim an der Ruhr.

* To whom correspondence should be addressed. E-mail: holzwarth@mpi-muelheim.mpg.de.

‡ Max-Planck-Institut für Strahlenchemie.

§ Università di Verona.

⊗ Abstract published in *Advance ACS Abstracts*, December 15, 1996.

[1] Abbreviations: A, antheraxanthin; Car, carotenoid; Chl *a* and *b*, chlorophyll *a* and *b*, respectively; CP 24, 26, and 29, chlorophyll−protein complexes of PS II; DADS, decay-associated absorption difference spectra; DM, *n*-dodecyl *β*-maltoside; ESA, excited state absorption; ET, energy transfer; HPLC, high-performance liquid chromatography; IEF, isoelectric focusing; L, lutein; LHC II, light-harvesting complex II; N, neoxanthin; PAGE, polyacrylamide gel electrophoresis; V, violaxanthin; Z, zeaxanthin.

S0006-2960(96)02467-1 CCC: $14.00

extensively in vitro (Frank et al., 1994; Ruban et al., 1993). With approximately C_{2h} symmetry, the absorption from the ground state to the S_2 state is strongly allowed while the S_1 state has a very low oscillator strength. True to their role as prospective quenchers, carotenoids are able to rapidly and nonradiatively dissipate excitation, mediated by vibronic coupling, predominantly to the C−C symmetric stretch vibrations (Frank et al., 1993). From studies of xanthophyll cycle carotenoids relevant to LHC II in vitro (Frank et al., 1994), the lifetimes of the S_1 states of V, A, and Z, repectively are 23.9, 14.4, and 9.0 ps. The S_2 state lifetimes are shorter and assumed to be on the same order as those of L (200−230 fs; Gillbro, unpublished results) and spheroidene (340 fs; Shreve et al. 1991). The lowest excited singlet level of Z (14 200 cm^{-1}) has been determined to lie below that of the Chl *a* excited singlet (14 700 cm^{-1}). In antheraxanthin, the corresponding singlet is essentially isoenergetic (14 700 cm^{-1}), while for V, it lies at higher energy (15 200 cm^{-1}). These relative energies appear to correlate well with the observation of inhibition and stimulation of fluorescence quenching by addition of V and Z, respectively, to trimers at low pH (Ruban et al., 1996). This is observed with greatest effect in CP 26 and 29 complexes and to a lesser extent in LHC II.

Rapid internal conversion and short excited state carotenoid lifetimes are the elements of an effective quenching mechanism, but this implies that conversely, for a carotenoid to behave efficiently as an antenna, the energy transfer rate must be high. Energy transfer may occur from the Car S_1 and S_2 states. Due to the very low oscillator strength of the S_1 state, energy transfer occurs via the Dexter mechanism (Razi Naqvi, 1980) or multipole Coulomb mechanism (Nagae et al., 1993). These mechanisms have different dependencies on pigment separation, although close proximity is necessary for efficient transfer. Alternatively, if the strongly allowed Car S_2 state is involved in energy transfer (Shreve et al., 1991), the Förster mechanism with a $1/R^6$ distance dependence may well be as efficient as or more efficient than transfer from the S_1 state, allowing greater separation between the pigments. These factors together with the relative energies of Car and Chl excited states provide the key to the antenna function of carotenoids in vivo.

In the advances toward understanding the function of LHC II, the electron diffraction structure (Kühlbrandt et al., 1994) has been central in interpretation of spectra and models. The structure of the trimeric complex has been resolved to 3.4 Å, but precise orientations of the pigments and the position of one of the three Cars have yet to be determined. Pigment analysis indicates at least seven Chl *a*, six Chl *b*, and three carotenoids per monomer. Since there is ultrafast transfer of energy from Chl *b* to Chl *a*, the Chl *a* should be most susceptible to triplet formation, and hence, the pigment assignment proposed by Kühlbrandt et al. assumes that all Chl *a* are located in close proximity to two central L Cars capable of quenching triplets. The remaining xanthophyll not resolved in the structure is expected to occupy a peripheral site.

Due to the close proximity between Car and Chl required for efficient energy transfer, the identity of Chls located closest to the Cars can be tested directly, in principle. A recent report (Peterman et al., 1995) addressed Chl triplet quenching by Cars in LHC II. They find evidence for triplet transfer from Chl *a* to three different Cars. This implicates the structurally unresolved peripheral xanthophyll, and this should also have consequences for singlet transfer. Here, we report on the role of LHC II Cars as antennas and present the results of singlet energy transfer from Car to Chl in LHC II with specific, well-determined Car compositions. The kinetics indicate preferential direct transfer from the central L to Chl *b*, not entirely consistent with the Kühlbrandt Chl assignment, as well as some Car to Chl *a* transfer in a mutant carrying a significant proportion of Z.

MATERIALS AND METHODS

Experiments have been run on LHC II trimers prepared from WT *Arabidopsis thaliana* and the ABA-3 mutant form, which is lacking the epoxidase that leads to the formation and interconversion of N, V, and A (Rock & Zeevaart, 1991). This mutant therefore contains only L and Z and lacks all other xanthophylls. Plants were grown for 5−6 weeks in a growth chamber with a 12 h/12 h light/dark cycle and a temperature of 25 °C in the light and 20 °C in the dark. Thylakoid membranes were isolated according to Bassi et al. (1985), washed with 0.8 M TRIS (pH 8.0), resuspended in distilled water at 2 mg of Chl/mL, and solubilized by adding DM to a final concentration of 1%.

LHC II was obtained by centrifuging the thylakoid membranes followed by preparative isoelectric focusing (Dainese & Bassi, 1991). The green bands with a p*I* between 3.6 and 3.9 were harvested, and the Chl proteins eluted from the gel with 50 mM Hepes (pH 7.6) and 0.06% DM. These bands were loaded onto a glycerol gradient and further separated by ultracentrifugation into three bands; the upper (yellow) contained free Cars and ampholytes from the IEF stage, the middle LHC II, CP26, and CP24, depending on the p*I*, and the third only trimeric LHC II as determined from SDS/PAGE, immunoblotting, and green gel analysis.

Critical for these measurements are LHC II samples with a well-determined and, as far as possible, uniform Car content. From careful HPLC analysis, the different isoforms of LHC II exhibited a very similar pigment composition, although small differences could be observed. To minimize heterogeneity, the femtosecond transient absorption measurements were performed with the most abundant isoforms showing a p*I* of 3.7−3.8 in both the wild type (WT) and the ABA-3 mutant. These preparations showed identical polypeptide compositions. Photosynthetic pigments were quantified with a modification of the method of Gilmore and Yamamoto (1991) using a Beckman 126 HPLC system equipped with a type 128 diode array detector. The total Chl concentration and the Chl *a*/*b* ratio were determined according to Porra et al. (1989). The pigment composition is given in Table 1.

Femtosecond transient absorption measurements have been performed using a titanium−sapphire oscillator/amplifier system producing 70−80 fs (FWHM) pulses at a repetition rate of 3 kHz (Holzwarth & Müller, 1996). The pulses were split, and a minor part was used to generate a white light continuum probe pulse. The major part was used to pump an optical parametric amplifier tuned around 500 nm to produce 60 fs pump pulses (FWHM) with a nearly transform-limited spectral width of roughly 4−5 nm (FWHM). A low excitation intensity of around 10^{13} photons cm^{-2} per pulse was used in each experiment, to reduce annihilation effects to a negligible level (Connelly et al., 1996).

A camera system (256-channel diode array with a resolution of 0.5 nm per channel, intrinsic rms noise level of 1 ×

Table 1: Pigment Composition of LHC II Fractions Purified from the Wild Type and ABA-3 Mutant[a]

sample	Chl *a*	Chl *b*	lutein	neoxanthin	violaxanthin	zeaxanthin	Chl *a*/*b*	Chl/Car
wild type LHC II	100	67	29.3	13.2	0.9	0	1.49	3.8
per monomer	7	5	2	1	trace	0	1.4	4.0
ABA-3 LHC II	100	67	19.5	0	0	8.6	1.49	5.9
per monomer	7	5	1.36	0	0	0.6	1.4	6.0

[a] The values are in moles of pigment per 100 moles of Chl *a*. The second and fourth rows show the pigment complement per LHC II monomer assuming that each polypeptide binds seven Chl *a* and five Chl *b* molecules.

10^{-5} ΔOD units) allowed the absorption changes in a 125 nm section of the white light spectrum to be detected simultaneously. Data were acquired over a 5 ps time range with a time resolution of 13.33 fs/point, for excitation wavelengths of 475, 490, and 515 nm and detecting in the carotenoid S_2 (<515 nm) as well as in the chlorophyll Q_y (630−700 nm) absorption regions. The samples had an optical density of 0.5−0.6 mm^{-1} at 675 nm and were contained in a 1 mm path length rotating, translating cuvette maintained at 4−6 °C.

RESULTS

The Chl *a*/*b* ratio in both WT and ABA-3 mutant LHC II samples is 1.49, closely fitting a total of seven Chl *a* and five Chl *b* molecules per LHC II polypeptide. The Car complement, on the contrary, differs: three in the WT and two in the ABA-3 mutant per polypeptide. This pigment composition, with particular reference to the Chl/Car ratio, was confirmed by matching the absorption spectrum of the LHC II pigments extracted in ethanol with a composite spectrum made up of individual pigments, purified by HPLC, in a comparable ratio. A composite spectrum with a ratio of 7/5/2/1 Chl *a*/Chl *b*/L/N most closely resembled that of the WT extract. In the case of the ABA-3 mutant, a ratio of 7/5/1.4/0.6 Chl *a*/Chl *b*/L/Z produced the most closely fitting composite spectrum. This difference of one in the total Car content presumably reflects disruption of the biochemical pathways dependent on the epoxidase in the mutant, although the precise mechanism is unknown (Rock & Zeevaart, 1991).

The Car composition of the two LHC II preparations suggests that in the WT, besides the two L molecules resolved in the LHC II by electron crystallography cross-bracing helices A and B (Kühlbrandt et al., 1994) assignment, a third Car site can be occupied either by N or in a trace of complexes by V. In the ABA-3 mutant, however, only two of these sites appear to be occupied, in a majority of complexes by L or otherwise by L and/or Z. A mixture of complexes containing either one or three Cars seems less likely. The problem of which of these sites is empty and therefore at the Z location thus arises. In vitro reconstitution studies on LHC II (Paulsen, 1995) and on the homologous complex CP 29 (Giuffra et al., 1996) have shown that L is essential for the stabilization of the LHC pigment−protein, which is consistent with its location in the two central sites resolved by electron diffraction. If this holds, then Z is located in one or both of the two central sites while the more peripheral one is empty. The alternative location for the Z in the third site is less likely but cannot be excluded.

To elucidate the individual roles of each Car in the energy transfer kinetics, it would be convenient to excite the individual carotenoids specifically. This cannot be achieved directly since all Cars absorb to varying degrees below 500 nm (Ruban et al., 1993). The possible exception is Z which appears to have the red-most absorption edge in the complex, indicated by a small positive signal in the ABA-3 mutant − WT difference absorption spectrum most clearly seen at 77 K. In view of this, we exploit the difference in Car constitution of the WT and ABA mutant and use several excitation wavelengths to try to distinguish the Car contributions. It is important to note however that vibrational and higher electronic states of Chl also make a large contribution to the absorption region at and below 500 nm. The difference between the fluorescence excitation (detected at 680 nm) and absorption spectra reflects the efficiency of energy transfer from Car to Chl and should be compared not with the total absorption but with the smaller contribution due to the Cars. This suggests an efficiency of less than 80−90%, which for unknown reasons is somewhat smaller than the 100% value obtained by Siefermann-Harms and Ninnemann (1982). The efficiency might well depend on the exact Car composition.

For femtosecond measurements, the WT LHC II was excited at 475 and 490 nm while the ABA-3 mutant was excited at 490 and 515 nm. In each case, the kinetics were measured around the Car S_2 region (∼500 nm) and the Chl Q_y region (∼630−700 nm)[2] and analyzed globally by fitting the kinetics of each spectral region to a sum of exponentials model. Dispersion effects were compensated by a linear correction (6 fs/nm in the Chl Q_y region) in the fit. The number of components necessary for a good fit were judged by the residuals and χ^2 values. The results for both the WT and ABA-3 mutant at each excitation wavelength are summarized in Table 2. Representative kinetics curves in the Chl Q_y region are given in Figure 1, showing a noise level of about 4×10^{-5} ΔOD units and good signal to noise. It can been seen directly from the curves that within the first 600 fs the kinetics should be described by a fast rise and a fast decay term, both with lifetimes of less than 300 fs.

Decay-associated absorption difference spectra (DADS) for the WT and ABA-3 mutant excited at 490 nm, where all Cars should have a pronounced absorption, are plotted in Figures 2a,b and 3a,b, respectively. These show similar characteristics. In the Chl region (Figures 2b and 3b), there appears to be little direct Chl excitation (≤10% of the final excitation) at zero time. In the Chl *b* region (640−660 nm), a rapidly rising component in the 100−200 fs range indicates that energy is transferred preferentially to Chl *b* on this time scale, concomitantly with an equally rapid prominant decay component in the Car absorption region (see Figures 2a and 3a). The significant difference between the WT and the ABA-3 mutant appears in the Chl *a* region (∼670−680 nm). In the WT, there appears to be a delayed rise (indicated by the negative amplitude of the fastest lifetime component),

[2] The kinetics data discussed in this paper presented as surfaces are available as Supporting Information.

Table 2: Summary of Global Analysis Results for the Wild Type and Mutant LHC II at Various Excitation Wavelengths

sample	excitation	lifetimes[a]	observation	inference
LHC II	490 nm		Chl region of 630−700 nm (less than 15% direct Chl excitation)	
wild type	(cf. Figure 2b)	142 fs	Chl *b* rise, max at 652 nm, Chl *a* bleaching max at 679 nm	Car−Chl *b* energy transfer
		245 fs	Chl *b* bleaching, Chl *a* rise max at 679 nm	Chl *b*−Chl *a* energy transfer
		2.5 ps	Chl *b* bleaching, Chl *a* rise max at 682 nm	Chl *b*−Chl *a* energy transfer
		3.6 ns[b]	Chl *b* ESA, Chl *a* bleaching max at 680 nm	equilibrated Chl relaxation
			Car region of 470−500 nm	
	(cf. Figure 2a)	141 fs	predominant bleaching component max at 488 nm	Car−Chl *b* energy transfer
		1.1 ps	bleaching component max at 489 nm	Chl kinetics
		3.6 ns[b]	near-zero bipolar component	Chl kinetics
LHC II	475 nm		Chl region of 630−700 nm (predominantly direct Chl b excitation)	
wild type	(cf. Figure 4)	123 fs	low-amplitude Chl *b* and Chl *a* rise max at 675 nm	Chl *b*−Chl *a* and Car−Chl *b*/ energy transfer
		394 fs	Chl *b* bleaching, predominant Chl *a* rise max at 679 nm	Chl *b*−Chl *a* energy transfer
		2.8 ps	bleaching at <678 nm, Chl *a* rise max at 683 nm	Chl *b*−Chl *a* energy transfer
		3.6 ns[b]	Chl *b* ESA, Chl *a* bleaching max at 680 nm	equilibrated Chl relaxation
			Car region of 470−500 nm	
		595 fs	bleaching component max at 485 nm	Chl kinetics
		4.4 ps	bleaching component max at 488 nm	Chl kinetics
		3.6 ns[b]	near-zero ESA component	Chl kinetics
LHC II	490 nm		Chl region of 630−700 nm (less than 15% direct Chl excitation)	
ABA-3	(cf. Figure 3b)	113 fs	Chl *b* rise max at 650 nm, Chl *a* rise max at 675 nm	Car−Chl *b*/*a* energy transfer
mutant		413 fs	Chl *b* bleaching, Chl *a* rise max at 679 nm	Chl *b*−Chl *a* energy transfer
		2.4 ps	Chl *b* and Chl *a* bleaching, Chl *a* rise at >675 nm and max at 682 nm	Chl *b*−Chl *a* energy transfer
		3.6 ns[b]	Chl *b* ESA, Chl *a* bleaching max at 681 nm	equilibrated Chl relaxation
			Car region 470−500 nm	
	(cf. Figure 3a)	105 fs	predominant bleaching component max at 488 nm	Car−Chl *b*/*a* energy transfer
		1.0 ps	bleaching component max at 488 nm	Chl kinetics
		3.6 ns[b]	low-amplitude zero crossing component	Chl kinetics
LHC II	515 nm		Chl region of 630−700 nm (predominantly direct and indirect Chl a excitation)	
ABA-3				
mutant	(cf. Figure 4)	60 fs	Chl *b* low-amplitude bleach, Chl *a* rise max at 673 nm	direct and Car−Chl *a* energy transfer
		390 fs	Chl *b* zero amplitude, Chl *a* rise max at 675 nm	Chl *a* equilibration
		1.7 ps	Chl *b* and Chl *a* bleaching, Chl *a* rise at >675 nm and max at 683 nm	Chl *b*/*a*−Chl *a* energy transfer
		3.6 ns[b]	Chl *b* ESA, Chl *a* bleaching max at 680 nm	equilibrated Chl relaxation
			Car region of 470−510 nm (beset by fast artifacts/oscillations)	
		173 fs[c]	predominant bleaching component max at 493 nm	Car−Chl *a* energy transfer
		1.15 ps	bleaching component max at 485 nm	Chl kinetics
		3.6 ns[b]	low-amplitude zero crossing component	Chl kinetics

[a] Lifetimes determined with a 10% error. [b] Fixed at the lifetime determined from fluorescence decay measurements. [c] An addional component around 50 fs was required to fit the fastest effects. These are largely due to stimulated resonance Raman effects but may mask a Car−Chl energy transfer component.

reflecting that energy transfers to Chl *a* mainly via Chl *b* and not directly from Car. By contrast, the ABA mutant also shows substantial Car to Chl *a* energy transfer, indicated by the 113 fs rise term in the Chl *a* region. Since both WT and ABA mutant complexes contain L which appears to transfer energy to Chl *b*, this difference in behavior appears to correlate with the presence of Z.

For all excitation wavelengths, components of a few hundred femtoseconds (250−600 fs) and a few picoseconds (2−4 ps) indicate Chl *b* to Chl *a* energy transfer. Due to the residual Chl absorption, small at 490 nm but more significant at 475 and 515 nm compared with the Car absorption, the Chl kinetics are reflected in the Car region DADS by the picosecond and nanosecond components which generally have lower amplitude than the main femtosecond Car decay component.

Spectra in the Chl absorption region obtained for excitation of the WT at 475 nm and the ABA-3 mutant at 515 nm at different delay times are illustrated in panels a and b of Figure 4, respectively. At both 475 and 515 nm, directly excited Chls contribute significantly to the absorption difference at zero time. Thus, at these wavelengths, with simultaneous Car to Chl and Chl *b* to Chl *a* energy transfer components with similar lifetimes of less than 200 fs (Connelly et al., 1996), the kinetics are less suited for a detailed analysis of the Car to Chl transfer. It is noteworthy though that at 515 nm excitation of the ABA-3 mutant there is still a discernible transfer from Car to Chl *a*, as observed at 490 nm, but almost no transfer to Chl *b*. This suggests that the red-most Car, probably Z in the ABA mutant, transfers predominantly to Chl *a*.

KINETIC ANALYSIS AND MODELING

Because exciting at 490 nm appears to lead to the minimum amount of direct Chl excitation (less than 15% of the total), only the kinetics observed following excitation at 490 nm are used to construct a minimal model for simulation. The WT kinetics, as illustrated in the DADS in figure 2a,b, show clearly that there is predominantly sequential energy transfer from Car to Chl *b* followed by slower Chl *b* to Chl *a* energy transfer. From the DADS, it is apparent that at least two Chl *a* pools[3] can be resolved at 679 and 682 nm. The Chl *b* region (640−660 nm) shows a broad spectral feature centered about 652 nm. This is considered to be due

[3] A pool in this context is defined as a spectrally limited range of pigment states or exciton levels that share a common kinetics (decay lifetime).

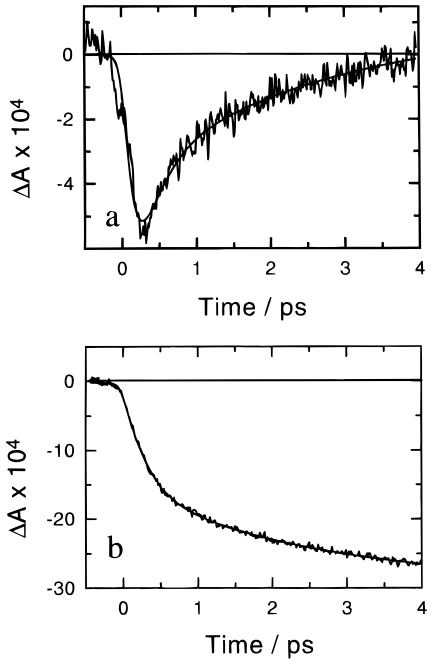

FIGURE 1: Representative kinetics curves for the WT LHC II exciting at 490 nm and recording at (a) 649 nm and (b) 681 nm (extracted from the camera data by binning over 3 nm). The noise level is about 4×10^{-5} ΔOD units and the signal to noise ratio roughly 10 at 649 nm and 50 at 681 nm.

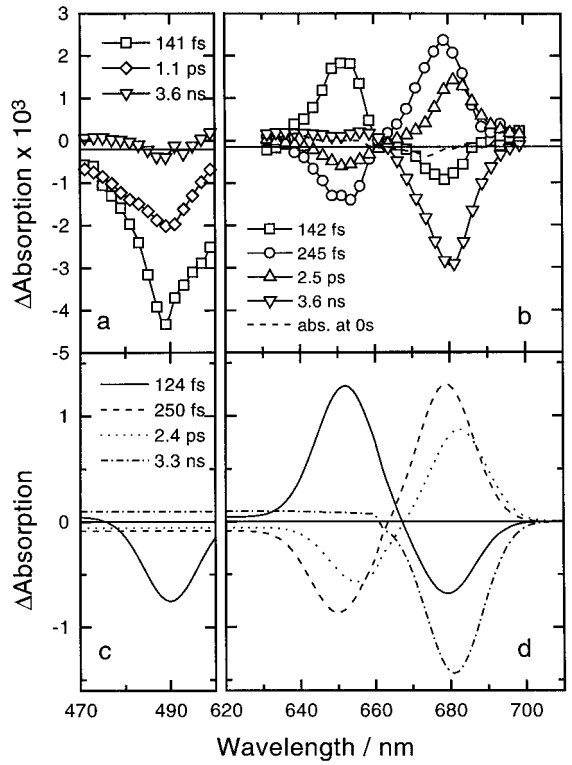

FIGURE 2: WT LHC II excited at 490 nm. (a) DADS from measured data in the Car S_2 region. (b) DADS from measured data in the Chl region. (c) Simulated DADS in the Car region. (d) Simulated DADS in the Chl region using the kinetic model in Scheme 1.

to at least two pools of Chl *b*: one centered at 650 nm (Chl *b*′) and transferring energy to the 679 nm Chl *a*′ pool and the other centered at 655 nm (Chl *b*″) transferring energy to the 682 nm Chl *a*″ pool. This is in reasonable correspondence with the kinetics and spectral detail observed by exciting at 650 nm (Connelly et al., 1996). In addition, there is equilibration between the Chl *a* pools, although this

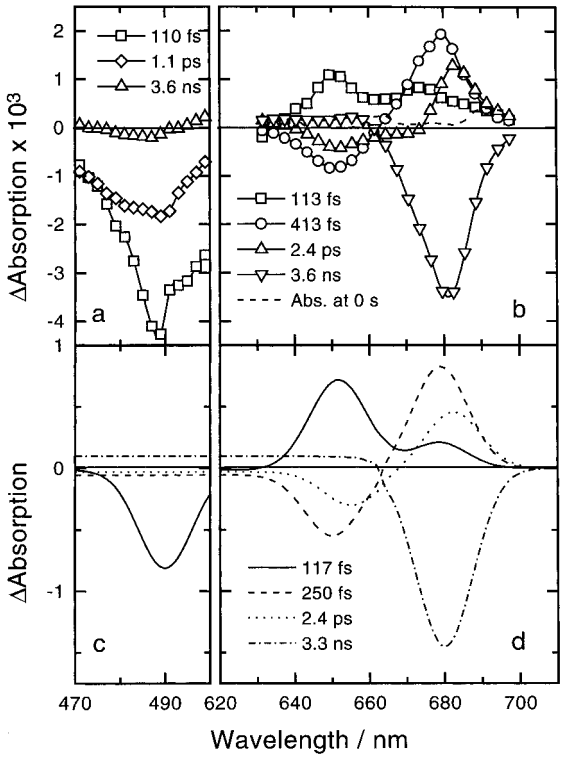

FIGURE 3: ABA mutant LHC II excited at 490 nm. (a) DADS from measured data in the Car S_2 region. (b) DADS from measured data in the Chl region. (c) Simulated DADS in the Car region. (d) Simulated DADS in the Chl region using the kinetic model in Scheme 2.

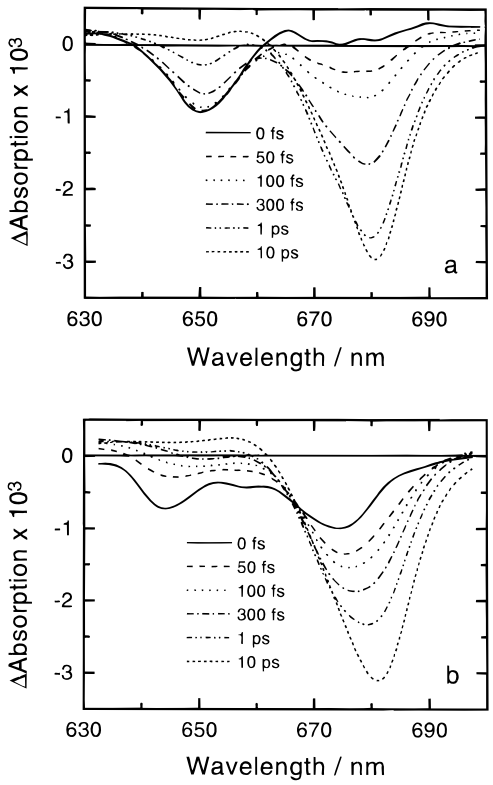

FIGURE 4: Difference absorption spectra of the Chl Q_y region of (a) the WT complex, excited at 475 nm, and (b) the ABA-3 complex, excited at 515 nm, at different delay times.

is not so clearly seen in the DADS (Figure 2b), suggesting that it occurs with a longer lifetime than the observed time frame (5 ps) or alternatively occurs very rapidly, on the same time scale as the fastest observed energy transfer processes.

Scheme 1

Wild type LHC II kinetic scheme

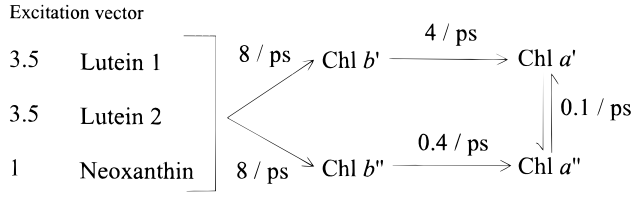

Scheme 2

ABA mutant LHC II kinetic scheme

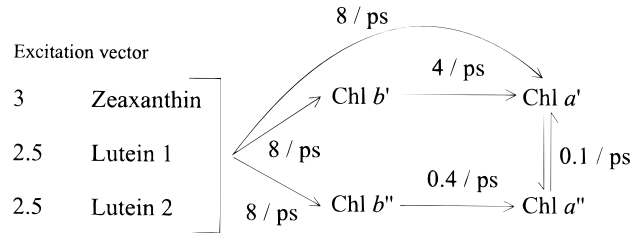

For the models presented here, the Chl *a* to Chl *a* energy transfer rate is assumed to be about 0.1 ps^{-1}.

The Car pool is considered to be centered at 490 nm and associated with the same Car to Chl *b* transfer rate for all Cars.[4] Light at 490 nm is expected to excite all Cars, and energy transfer to Chl is expected to occur from at least the two central Cars to be consistent with the 80−90% efficiency estimated from the fluorescence excitation spectrum. This appears to be consistent with the relative efficiency of energy flow into the Chl *a* spectral region in the ABA mutant observed by transient absorption measurements for a long time delay, following excitation at 490 and 650 nm (100% efficient). The proposed WT kinetic model is illustrated in the upper kinetic scheme. Relative amplitudes for the pools were assumed to be 0.8, 0.9, 1.5, 0.9, and 1.5 with Gaussian line widths (FWHM) of 20, 30, 30, 30, and 30 nm for Car (total), Chl *b*′, Chl *a*′, Chl *b*″, Chl *a*″, respectively. Some excited state absorption was included in the longest lifetime component to the blue of 665 nm. The closest simulation was obtained by assuming that the Car pool transfers to Chl *b*′ and Chl *b*″ in a ratio of 3.5, 4.5. If the Ls are assumed to behave similarly, then an excitation ratio of 3.5 for each L and 1 for N is reasonable where L2 and N transfer to Chl *b*″; in ethanol, the first absorption maximum of N below 500 nm lies further to the blue than for L (Ruban et al., 1993). Simulated DADS are illustrated in Figure 2c,d and can be compared directly with the observed DADS (Figure 2a,b). The relative amplitudes and positions of the maxima and minima in the Chl region are quite well reproduced with this simple model. No attempt has been made to simulate the Chl kinetics in the Car absorption region in detail.

The same kinetic scheme can be applied to the ABA-3 kinetics, but in this case, the scheme must be augmented with direct Car to Chl *a* energy transfer. It is assumed that the WT and ABA mutant show similar Car to Chl *b* energy transfer behavior due to the common central Ls. The observed difference in behavior is due to the presence of Z in the ABA-3 mutant, which promotes energy transfer to Chl *a*. The apparent heterogeneity of the ABA-3 mutant sample is accounted for in the excitation vector of the Cars and not by assuming specific structural details. Two serial energy transfer paths analogous to that of the WT, from Car to Chl *b* and then to Chl *a*, are retained in the ABA model. In addition, an energy transfer route direct from Car to Chl *a*′ is incorporated. The model is shown in the lower kinetic scheme. The closest correspondence between the observed and theoretical DADS is obtained when the Car pool is assumed to transfer energy to the Chl pools in a ratio 2.5/2.5/3 for Chl *b*′/Chl *b*″/Chl *a*′. If Z is assumed to transfer predominantly to Chl *a*′ directly, then an excitation ratio of 2.5 for L and 3 for Z may be assumed. The simulated DADS are illustrated in Figure 3c,d and can be compared directly with the observed DADS in Figure 3a,b. Again, the relative amplitudes, lifetimes, and shape of the DADS components are quite well reproduced with this simple model, particularly the 117 fs component which shows a rise across the Chl region in contrast to the analogous WT component.

DISCUSSION

The most startling result emerging from this study is the predominant sequential energy transfer from Car to Chl *b* and then to Chl *a* in the WT *Arabidopsis* LHC II trimers. The fact however, that there may be a minor (<10%) Car to short wavelength Chl *a* transfer contribution that cannot be distinguished from the kinetics cannot be dismissed however. Assuming the similarity between the WT and ABA-3 mutant complexes is due to conservation of the central Ls, energy transfer from the central luteins occurs preferentially to Chl *b*, a conclusion endorsed by our modeling studies. For efficient energy transfer from the Car S_1 state to Chl *b* by Dexter exchange (Shreve et al., 1991), the Car and Chl *b* should be in van der Waals contact. Pigment separations can be greater if energy transfers via the S_1 Coulomb and S_2 Förster mechanisms. However, an estimate of the transfer lifetime from the S_1 state gives 300 fs for 10 Å separation (Shreve et al., 1991) and from the S_2 state 250 fs for a 9 Å separation (Nagae et al., 1993). From the Kühlbrandt et al. (1994) pigment assignment, the L to Chl b center to center distances are 13 Å or more which, by either mechanism, results in a lifetime longer than our observed value of 142 fs for the WT. From the experimental kinetics, it is not possible to determine which mechanism is predominant. Further, it is important to note that, even if for a single Chl *b* the inverse transfer rate might be 150 fs, one would observe only a very small amount of energy transfer to Chl *b*, given a situation in which most Chl *a* were located much closer to the luteins, as the conventional assignment suggests. Thus, to overcome the competing effect of trapping by Chls *a* and to get the high efficiency of transfer to Chls *b* as observed, regardless of mechanism, about two Chls *b* must be located quite close to the Ls, implying positions currently assigned to Chl *a*, and this suggests a modification of the Chl assignment of Kühlbrandt et al. (1994) is necessary. A basic premise of the Kühlbrandt assignment that Chl *a* triplets are quenched by carotenoids has been confirmed in the triplet kinetic study of Peterman et al. (1995), and hence, some Chl *a* are known to be in close contact with the Cars. That these do not appear to contribute to the singlet energy transfer at 490 nm suggests these Chl *a* positions may be specifically

[4] Only one Car to Chl energy transfer rate is observed, and this is assumed to be the weighted averaged rate for all Cars, reflecting the fact that they have very similar and hence unresolved (in this study) individual rates.

optimized for efficient triplet transfer but not for singlet energy transfer, or may contribute to short wavelength Chl *a* pools not included in our minimal model.

The role of Z in the ABA mutant is also significant. It is not clear which position the Z occupies in the ABA mutant complex, although a central position would seem most likely. Close agreement between the kinetic model with the observed kinetics at 490 nm and the predominance of the Chl *a* kinetics at 515 nm suggests that Z acts as an antenna or promotes energy transfer predominantly to Chl *a*. It is also of interest to note that the WT and ABA mutant absorption spectra differ primarily in their Chl *b* and Car regions, an observation that has been confirmed more rigorously in difference spectra of reconstituted LHC II containing two different central Cars (R. Bassi et al., unpublished results). This would suggest either a direct interaction between the central Car and Chl *b* or a change in the protein−Chl *b* interaction induced by the presence of different Cars.

The precise Car to Chl energy transfer mechanism is unknown and may follow relaxation from Car S_2, which is expected to have a lifetime of a few hundred femtoseconds, to S_1 and then subsequently to Chl Q_y within the tens of picoseconds lifetime of the S_1 state, or via Car S_2 transfer to Chl Q_x followed by relaxation (Frank & Cogdell, 1996). Surprisingly, only one Car to Chl energy transfer rate for the different Cars is resolved in each complex, and the Car decay and Chl rise times are remarkably similar. It would be expected that these rates should depend critically on Car to Chl separations, and hence, some variation should be seen, within the lifetime of the S_2 state. However, with several Car to Chl and possible Chl *b* to Chl *a* processes occurring on roughly the same time scale, the observed lifetime represents a weighted average. Alternatively, the observed lifetime may correspond to the S_2 to S_1 Car relaxation which may be similar for each Car and implies that the S_1 lifetime for the Car to Chl energy transfer is even faster, i.e. $\ll$150 fs.

The differences in the Chl *b* to Chl *a* energy transfer component lifetimes ranging from 300 to 600 fs and 1.7 to 4.2 ps are an indication of the greater complexity of the Chl kinetics. In principle, each pigment pool will show multiexponential kinetics, although these will be dominated by the fastest processes. A weighted average of these is resolved in the observed kinetics which depends on the ratio of excitation. When excitation of Chl *b* is via the carotenoids, a greater selectivity might be obtained than by direct excitation at 650 nm (Connelly et al., 1996). The pool observed at 648 nm for excitation at 650 nm and correlating with a lifetime of 180 fs is not apparent in measurements at 490 and 515 nm, suggesting that this Chl *b* pool is either not excited or masked by Car to Chl *b* energy transfer. There is some evidence, particularly from the CP 29 complex, that the Chl *b* band at 640 nm is associated with Chl b_3 situated on helix D [notation of Kühlbrandt et al. (1994)] on the lumenal side of LHC II, near the C terminus (R. Bassi et al., unpublished results). Since there is no trace of the involvement of this Chl *b* in the kinetics, the peripheral Car, N, is probably located on the opposite side of the complex, near helix C. It is interesting to note that the features in the Chl *b* region are quite broad, centered at about 651 nm. The 1.7−4.2 ps component also shows variable spectral behavior; in particular, the position of its zero crossing ranges between 660 and 675 nm. This is in the Chl *a* region and probably represents variable extents of equilibration and localization among the pigments observable within the limited time frame used in these experiments (5 ps). With a better idea of the orientations and energy transfer among the Chls, provided by modeling for example, determination of the entry point for energy transfer from Car into the Chl network may allow the position of the unresolved Car to be determined, in the absence of direct structural data. This study provides the first steps toward determining the properties of Cars in LHC II by this means.

ACKNOWLEDGMENT

The authors thank Paolo Pesaresi for help in the preparation and characterization of the LHC II samples.

SUPPORTING INFORMATION AVAILABLE

Data describing the transient absorption measurements with LHC II for carotenoid excitation. This information is available only via the Internet. Ordering information is given on any current masthead page.

REFERENCES

Bassi, R., Machold, O., & Simpson, D. (1985) *Carlsberg Res. Commun. 50*, 145.

Bassi, R., Pineau, B., Dainese, P., & Marquardt, J. (1993) *Eur. J. Biochem. 212*, 297.

Bergantino, E., Dainese, P., Cerovic, Z., Sechi, S., & Bassi, R. (1995) *J. Biol. Chem. 270*, 8474.

Connelly, J. P., Müller, M. G., Hucke, M., Gatzen, G., Mullineaux, C. W., Ruban, A. V., Horton, P., & Holzwarth, A. R. (1996) *J. Phys. Chem.* (in press).

Dainese, P., & Bassi, R. (1991) *J. Biol. Chem. 266*, 8136.

Frank, H. A., & Cogdell, R. J. (1996) *Photochem. Photobiol. 63*, 257.

Frank, H. A., Farhoosh, R., Gosztola, D., Gebhard, R., Lugtenburg, J., & Wasielewski, M. R. (1993) *Chem. Phys. Lett. 207*, 88.

Frank, H. A., Cua, A., Chynwat, V., Young, A., Gosztola, D., & Wasielewski, M. R. (1994) *Photosynth. Res. 41*, 389.

Gilmore, A. M., & Yamamoto, H. Y. (1991) *J. Chromatogr. 543*, 137.

Giuffra, E., Cugini, D., Croce, R., & Bassi, R. (1996) *Eur. J. Biochem. 238*, 112.

Holzwarth, A. R., & Müller, M. G. (1996) *Biochemistry 35*, 11820.

Horton, P., Ruban, A. V., & Walters, E. A. (1996) *Annu. Rev. Plant Physiol. Plant Mol. Biol. 47*, 655.

Jennings, R. C., Bassi, R., & Zucchelli, G. (1996) *Top. in Curr. Chem. 177*, 147.

Kühlbrandt, W., Wang, D. N., & Fujiyoshi, Y. (1994) *Nature 367*, 614.

Nagae, H., Kakitani, T., Katoh, T., & Mimuro, M. (1993) *J. Chem. Phys. 98*, 8012.

Paulsen, H. (1995) *Photochem. Photobiol. 62*, 367.

Peterman, E. J. G., Dukker, F. M., van Grondelle, R., & Van Amerongen, H. (1995) *Biophys. J. 69*, 2670.

Porra, R. J., Thompson, W. A., & Kriedemann, P. E. (1989) *Biochim. Biophys. Acta 975*, 384.

Razi Naqvi, K. (1980) *Photochem. Photobiol. 31*, 523.

Rock, C. D., & Zeevaart, J. A. D. (1991) *Proc. Natl. Acad. Sci. U.S.A. 88*, 7496.

Ruban, A. V., Horton, P., & Young, A. J. (1993) *J. Photochem. Photobiol. B 21*, 229.

Ruban, A. V., Young, A. J., & Horton, P. (1996) *Biochemistry 35*, 674.

Shreve, A. P., Trautman, J. K., Frank, H. A., Owens, T. G., & Albrecht, A. C. (1991) *Biochim. Biophys. Acta 1058*, 280.

Siefermann-Harms, D., & Ninnemann, H. (1982) *Photochem. Photobiol. 35*, 719.

BI962467L